Talanta 218 (2020) 121153

Contents lists available at ScienceDirect

Talanta

journal homepage: www.elsevier.com/locate/talanta

Microbial nanocellulose adherent to human skin used in electrochemical sensors to detect metal ions and biomarkers in sweat

Robson R. Silva[a,1,*], Paulo A. Raymundo-Pereira[a,1], Anderson M. Campos[b], Deivy Wilson[a], Caio G. Otoni[c], Hernane S. Barud[d], Carlos A.R. Costa[e], Rafael R. Domeneguetti[f], Debora T. Balogh[a], Sidney J.L. Ribeiro[f], Osvaldo N. Oliveira Jr.[a]

[a] São Carlos Institute of Physics, University of São Paulo (USP), São Carlos, 13566-590, São Paulo, Brazil
[b] São Carlos Institute of Chemistry, University of São Paulo (USP), São Carlos, 13566-590, São Paulo, Brazil
[c] Institute of Chemistry, University of Campinas (UNICAMP), P.O. Box 6154, Campinas, 13083-970, São Paulo, Brazil
[d] Biopolymers and Biomaterials Laboratory (BIOPOLMAT), University Center of Araraquara (UNIARA), Araraquara, 14801-340, São Paulo, Brazil
[e] Brazilian Nanotechnology National Laboratory (LNNano), Brazilian Center for Research in Energy and Materials (CNPEM), Campinas, 13083-861, São Paulo, Brazil
[f] São Paulo State University (UNESP), Department of General and Inorganic Chemistry, Rua Professor Francisco Degni, 55, Araraquara14800-060, São Paulo, Brazil

ARTICLE INFO

Keywords:
Bacterial cellulose
Wearable electronics
Biosensor
Heavy metals
Uric acid
Estradiol

ABSTRACT

The pursuit of biocompatible, breathable and skin-conformable wearable sensors has predominantly focused on synthetic stretchable hydrophobic polymers. Microbial nanocellulose (MNC) is an exceptional skin-substitute natural polymer routinely used for wound dressing and offers unprecedented potential as substrate for wearable sensors. A versatile strategy for engineering wearable sensing platforms is reported, with sensing units made of screen-printed carbon electrodes (SPCEs) on MNC. As-prepared SPCEs were used to detect the toxic metals cadmium (Cd^{2+}) and lead (Pb^{2+}) with limits of detection of 1.01 and 0.43 μM, respectively, which are sufficient to detect these metal ions in human sweat and urine. SPCEs functionalized through anodic pre-treatments were used for detecting uric acid and 17β-estradiol in artificial sweat, with detection limits of 1.8 μM and 0.58 μM, respectively. The electrochemical treatment created oxygen groups on the carbon surfaces, thus improving wettability and hydrophilicity. MNC was herein exploited as an adhesive-free, yet highly skin-adherent platform for wearable sensing devices that also benefit from the semi-permeable, non-allergenic, and renewable features that make MNC unique within the pool of materials that have been used for such a purpose. Our findings have clear implications for the developments on greener and more biocompatible but still efficient substrates and may pave the route for combining immunosensing devices with drug delivery therapies.

1. Introduction

As the largest and fastest-growing organ of the human body, the skin is a suitable interface for noninvasive detection of vital signs, such as blood pressure, oxygen intake, electrodermal activity, and temperature [1]. It also offers an interface to sweat, a water-rich fluid secreted by apocrine and eccrine glands in the epidermis during human perspiration primarily designed to regulate the body temperature. Sweat carries a library of biomarkers such as electrolytes, sugars, amino acids, proteins, hormones, and metabolites [2,3], whose levels may be useful to investigate athlete performance [4–6], diagnose genetic disorders and infections [7], and identify illicit drug metabolites [3,8]. The use of sweat for noninvasive detection is not new [9], but traditional analyses still rely on tedious collection procedures (e.g., swabbing the skin or collecting fluid with a microsyringe under induced sweating). Other limitations are related to storage, use of benchtop equipment, and obsolete protocols that introduce analytical errors and restrict the number of analyzed samples. Significant efforts have been made to design miniaturized devices [10] to quantify electrolytes, biomarkers, hormones, and harmful species in sweat using optical [11,12] and electrochemical signals [5]. These efforts have led to wearable point-of-care devices in different formats, e.g. patches, clothing, wristbands [2,7,13], rings, tattoos [10,14], including a few commercial epidermal microfluidic lab-on-a-chip devices such as ECHO® Monitor, Embrace®, Biolinq®, and Xsensio®. A review on wearable sweat sensors is found in Bariya et al. [12].

* Corresponding author.
E-mail addresses: rosa@chalmers.se, robsilva31@usp.br (R.R. Silva).
[1] These authors contributed equally to this work.

https://doi.org/10.1016/j.talanta.2020.121153
Received 20 January 2020; Received in revised form 7 May 2020; Accepted 9 May 2020
Available online 19 May 2020
0039-9140/

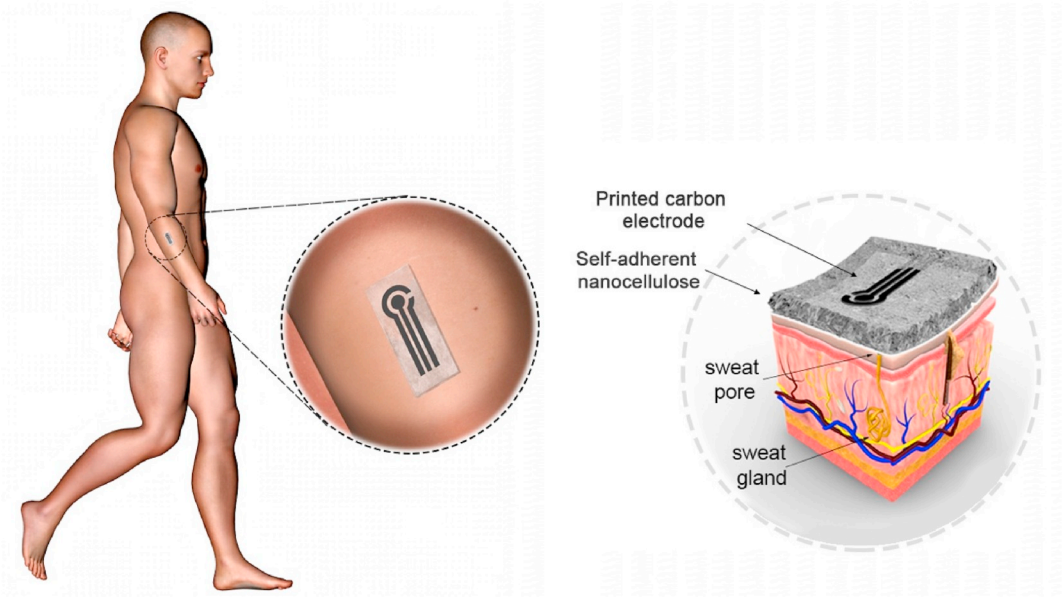

Fig. 1. Representation of a sensor made with a screen-printed carbon electrode deposited on a microbial nanocellulose substrate, alongside skin integration for noninvasive detection of biomolecules in biological fluids.

The concentration of biomarkers in sweat is expected to be low, thus requiring very sensitive principles of detection. Electrochemical sensors may fulfill this requirement for they can detect analytes at parts per billion (ppb) or even parts per trillion (ppt) levels, in addition to providing fast response, reproducibility, and long-term stability [1,2,4,7,9,10,13]. Skin-like electrochemical sensors have been built on biocompatible, soft, and flexible synthetic polymers that enable optimal conformal skin-contact devices. Use has been made of silicone materials (e.g., poly(dimethylsiloxane) (PDMS), Ecoflex, and Solaris), poly(vinyl alcohol) (PVOH), poly(ethylene terephthalate) (PET), poly(ethylene naphthalate) (PEN), Silbione®, acrylic tapes, polyimide, and polyester [15]. These polymers exhibit similar elastic moduli compared to skin, but they prevent transpiration and lack adhesion when used as substrates [12]. Using additional adhesives increases the probability of skin irritation and dermal stress due to the overall poor air permeability, restricted water drainage, and limited diffusion of analytes from sweat [16,17]. Such limitations can be overcome with natural polymers such as collagen, hyaluronic acid, gelatin, and cellulose. In fact, lignocellulosic plant fibers are the most ancient fabric material to wear the human skin [18].

Cellulose can be obtained from various sources, including microbial nanocelluloses (MNCs) produced by bacteria (e.g., *Acetobacter xylinum* and *Pseudomonas*) through oxidative fermentation in synthetic and non-synthetic media. MNCs consist of sophisticated web-like networks of ribbon-shaped pure cellulose nanofibrils with diameters smaller than 100 nm, which are themselves an assembly of numerous 2-4-nm-diameter nanofibrils. Unlike plant-derived nanocelluloses, MNCs are devoid of lignin and hemicellulose, offering superior mechanical properties and high porosity and permeability to liquids [19]. MNCs are available as ordinary medical products in the form of adhesive-free wound-dressing membranes and scaffolds for regenerating soft and hard tissues (e.g., bone, skin, and cartilage) and as artificial blood vessels for microsurgery and as dental implants [20,21]. Mass production with 500–1500 tons annually per producer can be achieved in traditional fermentation industry of *nata de coco* farms situated in Asian countries, especially Philippines, Indonesia, Vietnam, and Thailand [22–24]. MNCs are retrieved as millimeter-thick layers of swollen gel, which upon drying shrink laterally into sheets with thickness of a few microns. Moistening the sheet does not recover the gel state; instead, the sheet-like characteristics are maintained. These sheets have unique properties such as relative chemical inertness, solvent resistance (i.e., insolubility in water and most organic and inorganic solvents), high mechanical strength, small thermal expansion coefficient, and possibility of shaping into different morphologies.

With regard to wearable devices, MNCs may be advantageous as they are biocompatible with human tissues and nearly non-degradable in the body due to their high degree of crystallinity and because humans lack enzymes that break their β-(1,4) glycosidic linkages. Since MNC morphology mimics the nanoscale architecture of the native extracellular matrix (ECM), they have been investigated as temporary substrate for the adhesion and growth of skin cells for extensive burns and skin damaged by mechanical traumas or chronic ulcers [25–27]. Dried MNC membranes display permeability for liquids and gases [28] and low skin irritation alongside adhesive-free adherence to skin moisture [25–27]. With such properties, MNC membranes have been used as matrices to host optically active species to detect thiourea [29], cyanide [29], biothiols (cysteine, glutathione and cysteamine) [30], iodide and methimazole iodide [29,31], hydrogen peroxide [32,33], *E. coli* [34], UV light [35], and mechanical stress [36].

To the best of our knowledge, it has not been explored as a substrate for electrochemical detection of analytes in body fluids. Given its high purity compared to plant-derived paper [37], MNC (i.e., cellulose and water) stands out as an excellent substrate for wearable (skin-like) electrochemical devices that are lightweight, disposable, biodegradable, and capable of absorbing and percolating fluids by capillarity action. Moreover, MNC displays a nonresponsive background either in aqueous or non-aqueous analyses. Due to their nature, MNC dried sheets are inherently robust with very low density, and more hydrophilic with low barrier properties (e.g. high water absorption capacity, high water vapor and oxygen transmission rate) than plastic substrates used in wearable technologies (see a comparison of figures of merit in the Supporting Information, Table S1). Hence MNC should be suitable for breathable substrates. Herein, we demonstrate the application of MNC sheets as proof-of-concept skin-like platforms for noninvasive monitoring of body fluids in sweat. Fig. 1 illustrates the concept where a wearable SPCE built on MNC sheet is attached to human skin. To demonstrate the SPCE's suitability for various sensing modalities, we detected toxic metals (Cd^{2+} and Pb^{2+}), uric acid, and 17β-estradiol

across physiologically relevant concentration ranges. The relevance of these analytes is highlighted when the corresponding results are presented.

2. Materials and methods

2.1. Materials

The strain used to grow the bacterial cellulose hydrogel was *Gluconacetobacter xylinum* (ATCC 23769) supplied by André Tosello Foundation (Campinas, Brazil). Anhydrous D-glucose, yeast extract 4% (w/v), magnesium sulfate heptahydrate, ethanol (99.8%), and anhydrous potassium phosphate monobasic were purchased from Synth (São Paulo, Brazil). Deionized ultrapure water (resistivity > 18 MΩ cm) from a Milli-Q system (Barnstead Nanopure Diamond, Van Nuys, USA) was used is all experimental procedures. For the preparation of artificial sweat, lead nitrate (99%), cadmium nitrate (99%), 17β-estradiol (99%), uric acid (99%), urea (99%), potassium chloride (99%), sodium chloride (98%), sodium phosphate dibasic (99%), sodium phosphate monobasic monohydrate (99%), and lactic acid (85%) were acquired from Sigma-Aldrich (St. Louis, USA) with analytical grade and high purity. Sulfuric acid (96%) was obtained from Merck (New Jersey, USA). Carbon paste (BQ221) was purchased from Dupont (Wilmington, Delaware, USA). Analytical grade chemicals were used as received.

2.2. Microbial nanocellulose

G. xylinum was grown in 30 × 60 cm^2 plates during 96 h at 28 °C. We used as growth medium 0.7 L of an aqueous solution of glucose (50 g L^{-1}), yeast extract (4 g L^{-1}), KH_2PO_4 anhydrous (2 g L^{-1}), and $MgSO_4{\cdot}7H_2O$ (0.72 g L^{-1}) after sterilization by autoclaving at 121 °C and 1 (atm) kgf·cm^{-2} for 20 min and then added by 20 mL of ethyl alcohol. The hydrated MNC membranes were immersed in 0.1 M NaOH solutions at 80 °C for 45 min and then washed with distilled water several times until pH 7. MNC membranes were stored dipped in distilled water at 5 °C until further use. To serve as substrates for SPCEs, MNC membranes were slightly stretched using polytetrafluoroethylene holders and kiln dried at 60 °C.

2.3. Electrode fabrication

The SPCEs were fabricated over a dried MNC substrate using a semi-automatic screen printer, model INDEX INB (IMAH Indústria de Máquinas Ltda, Pinhais, Brazil) and the appropriate stencil was designed in AutoCAD version 2018 (Autodesk Inc., San Rafael, USA) and outsourced for fabrication on 150-mesh polyester screens. A carbon layer was deposited onto MNC using a pattern comprising the electrical contacts and working and counter electrodes. Then, the sheet with SPCEs was placed in an oven at 90 °C for 30 min, allowing for complete drying of the paste solvent. Carbon paste BQ221 was selected owing to its performance as working electrode for highly sensitive SPCEs biosensors [38,39]. It consists of a thermoplastic resin, conductive carbon particles (e.g. graphite flakes and carbon black, etc.) with a solid composition of 32 wt%, and a solvent (its chemical composition is proprietary of the manufacturer).

2.4. Determination of toxic metals, uric acid, and 17β-estradiol analytes

Phosphate buffer solution (PBS; pH 7.0) containing sodium phosphate dibasic and sodium phosphate monobasic monohydrate at 0.1 mol L^{-1} was used as electrolytic solution. Quantifications of toxic metals, UA, and 17β-estradiol in synthetic sweat samples were performed as in a previous work [40], with synthetic sweat consisting of urea (1.0 g L^{-1}), KCl (1.0 g L^{-1}), NaCl (7.5 g L^{-1}), and lactic acid (1.0 mL L^{-1}) solubilized in PBS. The limits of detection (LOD) were calculated with $LOD = a + 3Sy/x$ with a and Sy/x being the intercept and the standard deviation of the linear regression [41,42] respectively.

SPCEs were activated by immersing in H_2SO_4 0.1 mol L^{-1} for 60 s. An anodic potential of +2.5 V was applied for additional 60 s. The SPCE was washed with ultrapure water and immersed in phosphate buffer at pH 7.0. Fresh aqueous solutions of uric acid or 17β-estradiol were prepared in phosphate buffer (pH 7.0) before the measurements. Firstly, ten differential pulse voltammetry (DPV) scans were performed in phosphate buffer followed by addition of appropriate amounts of fresh solutions to obtain the final concentrations. All electrochemical data were recorded in a potentiostat/galvanostat, model Metrohm Autolab PGSTAT302 N (Eco Chemie, Utrecht, Netherlands) controlled by NOVA software. The experiments were carried out using a three-electrode configuration (i.e., working electrode, counter electrode, and reference). The following differential pulse voltammetry parameters were used: potential range: −0.4 to 0.6 V; step: 1.05 mV; modulation amplitude: 50 mV; modulation time: 0.05 s; and interval time: 0.2 s.

2.5. Characterization

Scanning probe microscopy experiments were carried out in FlexAFM scan head, I100 scan head interface, and C3000 controller (Nanosurf, Liestal, Switzerland) with the Kelvin probe force microscopy (KPFM) functionality. An additional external lock-in Stanford (SR830) was set to couple the amplitude signal with a simple linear dependence to tip-sample capacitance ($\partial C/\partial z$) in a single pass scanning. The scan head was mounted within a homemade environmental chamber that allows controlling both relative humidity (RH) and temperature (30% RH and 25 °C). Atomic force microscopy (AFM) images were acquired using Pt/Ir coated Si tip cantilevers - PPP-EFM (NanoSensors, Neuchâtel, Switzerland). Electron microscopy images were taken in a Zeiss Sigma (Zeiss, Oberkochen, Germany) scanning electron microscope equipped with a field emission electron gun (SEM-FEG) operating at 20 kV to analyze film homogeneity. The contact angle measurements were performed in three samples by dropping 3 μL of PBS solution onto the substrate using the sessile drop technique with a CAM200 goniometer (KSV Instruments, Helsinki, Finland). Electrode samples were analyzed by X-ray photoelectron spectroscopy (XPS) on a K-Alpha spectrometer (ThermoFisher Scientific, Waltham, USA) operating with monochromatic Al Kα radiation. Survey spectra were acquired using a pass energy of 200 eV and a 300-μm spot size at two random spots within each sample. High-resolution spectra were recorded in the regions assigned carbon and oxygen using a pass energy of 50 eV. Thirty scans were acquired and averaged per sample, and at least two samples per treatment were analyzed. XPS data were processed using the ThermoAvantage software, version 5.921 (ThermoFisher Scientific, Waltham, USA). Infrared spectroscopy was performed using Bruker Optics-Vertex 70 V spectrometer equipped with accessory A225/Q Platinum ATR, Multiple Crystals CRY:Diamond for attenuated total reflectance measurements. The transmission spectra were recorded in 128 scans at a resolution 4 cm^{-1} in the region of 4000–400 cm^{-1}. The Raman spectra were measured in a micro-Raman spectrometer (LabRAM Horiba Jobin Yvon-model HR 800), equipped with a He–Ne laser at 632.81 nm (17 mW) and a CCD camera. The measurements were performed in backscattering configuration with 50 × WD objective (Olympus MPL) by exposing the samples during 30 s of acquisition time for three accumulation intervals. The slit width of the Raman spectrometer was 100 μm and a diffraction grating of 600 lines/mm was used. The laser conditions were chosen to avoid damage of the material during the analysis.

3. Results and discussion

3.1. Screen-printed carbon electrodes on microbial nanocellulose substrates

The electrochemical wearable sensors were designed herein with a three-electrode configuration (i.e., working electrode, counter

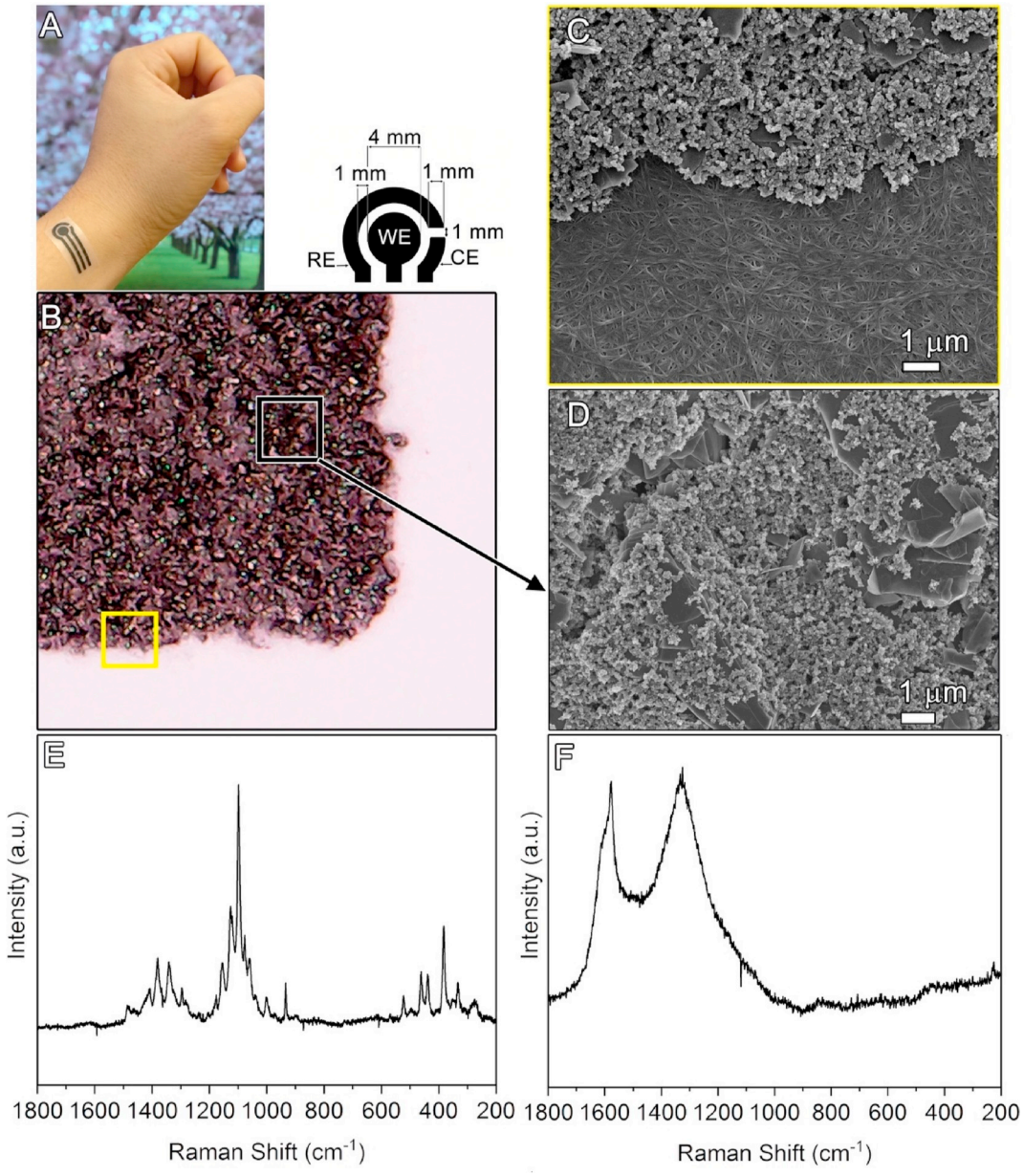

Fig. 2. Photograph of screen-printed carbon electrodes on microbial nanocellulose (MNC) adhered on skin and the corresponding dimension (A). Optical micrograph of an electric contact edge on a screen-printed carbon electrode (SPCE) (B). The yellow and black squares highlight the interface of MNC/carbon paste and SPCE surfaces, respectively. SEM images of the interface of MNC/carbon paste (C) and working SPCE (D) surfaces. Raman spectra of MNC (E) and regular SPCE over a MNC sheet (F). (For interpretation of the references to colour in this figure legend, the reader is referred to the Web version of this article.)

electrode, and reference) and screen-printed on the surface of dried MNC sheets. The carbon ink used was a commercial conductive ink made of pyrolytic carbon (i.e., graphite and carbon black) and a polymer binder. The screen-printed carbon electrodes (SPCEs) can be mass-printed at micrometric resolution delivering sensors with high sensitivity and selectivity at relatively low cost (below 1¢ per unit). As-produced SPCEs on MNC substrates are shown in Fig. 2A, where each unit contains the working, auxiliary, and reference electrodes. The edge of an electric contact in an electrode is shown in Fig. 2B, while Fig. 2C and 2D show SEM images of bare MNC and SPCE surfaces, respectively. Carbon flakes and carbon black nanoballs are seen on MNC, and SPCE had isolated, irregularly shaped graphite flakes. The coating of MNC sheets with carbon paste was further confirmed with Raman scattering spectroscopy by monitoring the typical D-band and G-band in carbon nanomaterials (Fig. 2E and 2F) and the changes in the fingerprint region of cellulose chain vibrational bands in the FTIR spectra of MNC (Fig. S1). The assignment of infrared and Raman bands is depicted in Table S2. Fig. 2E does not show such bands for a pristine MNC sheet, which are present in Fig. 2F for the SPCE surface at 1325 cm^{-1} (D-band due to the structural disorder in sp^2 hybridized carbon) and at 1577 cm^{-1} (first-order G-band).

3.2. Determination of toxic metals in sweat

Cd^{2+} and Pb^{2+} have been quantified in previous works at higher concentrations in sweat than in blood plasma or urine [43]. A brief description of the current source of contamination of Pd^{2+} and Cd^{2+} in everyday products and toxicological aspects in the human body is presented in the Supporting Information. In this work, we explored differential pulse anodic stripping voltammetry (DPASV) to detect Cd^{2+} and Pb^{2+} simultaneously in artificial sweat using SPCEs on MNC substrates. Stripping analysis is the most sensitive, effective

electroanalytical technique because it relies on two steps: a) prior accumulation step at which Pb^{2+} and Cd^{2+} are deposited on the electrode under convective mass transport; and b) measuring step at which the species are 'stripped away' from the electrode, producing a current proportional to their concentration.

3.2.1. Effect of experimental variables

3.2.1.1. Pre-concentration potential and time. The parameters accumulation potential and time for pre-concentration were optimized as shown in Fig. S2 using Cd^{2+} at 45 μM in artificial sweat. For an accumulation potential of −0.4 V, reduction of Cd^{2+} was not observed in the range of potential from −1.20 to 0.20 V. The peak current assigned to Cd^{2+} increased at accumulation potentials from −0.8 to −1.2 V because the potential is converging to the reduction potential of Cd^{2+}. However, the peak current decreased at −1.4 V as it is near the electrochemical reduction potential of other species, such as hydrogen ions, which in turn affect Cd^{2+} reduction and electrode stability. Moreover, since the accumulation potential was −1.4 V and DPV started at −1.2 V, there was redissolution of Cd^0 from the electrode surface. For the accumulation time survey, −1.2 V was selected as the standard accumulation potential because it delivered higher anodic currents. After 120 s, the slope slightly decreased because of the rapid surface saturation and the peak became distorted and broadened, influencing LOD and sensitivity. Therefore, 120 s was chosen as the optimal accumulation time to obtain LOD for low concentrations of Pb^{2+} and Cd^{2+} ions.

3.2.2. Simultaneous detection of Cd^{2+} and Pb^{2+} in artificial sweat

Fig. 3A and 3B shows successful detection of Cd^{2+} and Pb^{2+} in synthetic sweat in the ranges between 4.5 and 14.5 μM and from 1.0 to 10.5 μM, respectively, using as-prepared SPCEs. The anodic peak current increased linearly with the metal concentration according to DPASV data in Fig. 3B. The equations of linear regression of the analytical curves are: $I\ (A) = 8.5 \times 10^{-6} + 0.07\ C_{Cd2+}$ (M) and $I\ (A) = 8.6 \times 10^{-6} + 0.3\ C_{Pb2+}$ (M), wherein I is the current in A, and C_{Cd2+} and C_{Pb2+} are molar concentrations of Cd^{2+} and Pb^{2+}. The detection limits are 1.01 and 0.43 μM, respectively. Also, Cd^{2+} and Pb^{2+} could be detected individually in sweat, with sensitivity and detection limits of 0.07 and 0.3 A M^{-1} and 0.8 and 0.6 μM, respectively. This performance means that SPCEs on MNC are sufficient to apply for human sweat and urine, even considering the low physiological levels of heavy metals in human sweat and urine (< 1 mg L^{-1}) [43–46].

Table 1 shows a list of previous works with SPCEs on flexible substrates to detect Pb^{2+} and Cd^{2+} in different matrices using stripping voltammetry. We could not find any report on the use of skin-like SPCE for detection of toxic metals (i.e., Pb^{2+} and Cd^{2+}) in sweat. The LOD of as-prepared SPCE for Pb^{2+} and Cd^{2+} in artificial sweat in this work is higher than in previous studies using different matrices, which may be attributed to the following reasons: a) given the nature of nanofibrils, MNC is a potential adsorbent for toxic metal ions, which might seem as a disadvantage compared to (synthetic) plastic or ceramic substrates. However, MNC is a highly adherent biocompatible skin-like platform that can transport species such as toxic metals from sweat to the printed carbon ink through capillary effect; b) MNC sheets swell when immersed in polar solvents, especially aqueous solutions, which may cause a deleterious effect on the electrical signal (i.e., measured current) due to broadening of conductive tracks width and raise of microcracks; c) SPCE is electrochemically less active and selective because of its polymeric material that restricts electron transfer at the electrode-electrolyte interface and minimizes electron transfer kinetics [47].

3.3. Detection of uric acid and 17β-estradiol

Uric acid and 17β-estradiol are relevant biomarkers, for they are related to medical disorders and health conditions. In the Supporting Information we provide the motivation for having chosen these biomarkers for our proof-of-principle experiments. We first tried to detect UA and 17β-estradiol with bare SPCEs, but the sensing performance was poor due to the low conductivity since there were few redox active sites on the carbon surface. Then, we resorted to electrochemical pre-treatments often applied to activate carbon paste by removing solvents and residues from printing through electrochemical processes [5]. Anodic pre-treatment usually enhances the electroactivity by increasing the density of oxygenated groups on the SPCE surface, improving the electron transfer rate. We investigated if anodic pre-treatment the SPCE surface printed on MNC sheets could enhance the sensitivity, and thus enable detection of uric acid and 17β-estradiol. Cyclic voltammetry was used to study the electrode surface upon such pre-treatment. SPCEs were submitted to +2.5 V during 60 s, and the results in Fig. 4 indicate that the treatment did affect the separation between the oxidation and reduction peaks, with ΔEp ≈715 and 663 mV *vs.* Ag/AgCl for bare and anodically pre-treated SPCEs, respectively. A highest current density was observed for the electrodes submitted to the anodic procedure, thus leading to the smallest charge-transfer resistance (R_{ct}) in the Nyquist plots in Fig. 4C and 4D, where R_{ct} values were 1.54 and 0.09 for bare and anodically pre-treated surfaces, respectively. It is hypothesized that co-products in the ink were removed from the surface upon anodic treatment due to the generation of molecular oxygen (O_2) on the carbon surface during the electrochemical reaction. We also evaluated the performance of SPCE electrodes after cathodic pre-treatment, where they were submitted to −2.5 V during 60 s. The SPCEs submitted to cathodic pre-treatment display ΔEp ≈659 mV *vs.* Ag/AgCl, which is similar to ones submitted to anodic pre-treatment, and an intermediated Rct of 0.89 kΩ as shown in Fig. S4. Small differences among

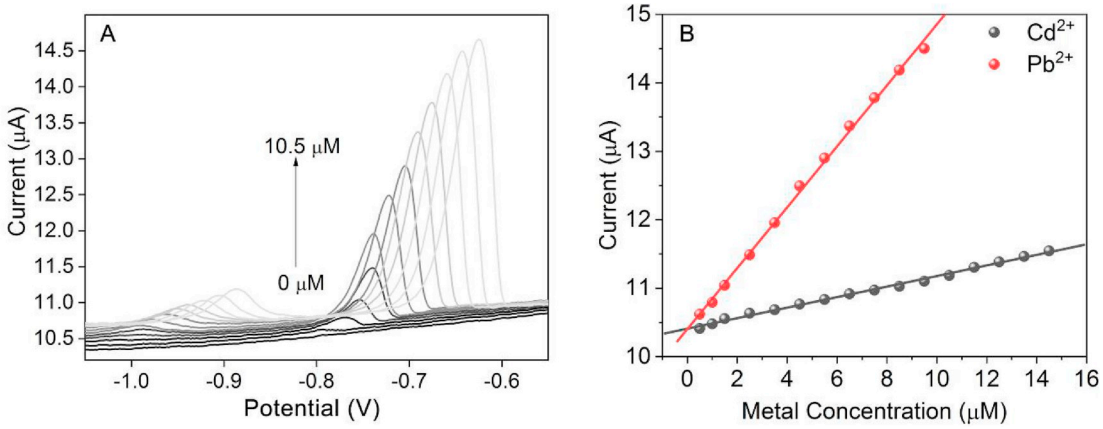

Fig. 3. Differential pulse adsorptive stripping voltammetry (A) and analytical curves for the simultaneous detection of Cd^{2+} (4.5–14.5 μM) and Pb^{2+} (1.0–10.5 μM) in sweat (B) using bare screen-printed carbon electrodes.

Table 1
Figures of merit for determination of Pb^{2+} and Cd^{2+} using SPCEs. Due to the limited studies on SPCE for detection of Pb^{2+} and Cd^{2+} on relevant biological fluids, figures of merit for environmental purposes are also included.

Modification	Substrate	LOD (μM)	Linear range (μM)	Sample	Ref.
Pristine graphite ink	Plastic	Pb^{2+} = 0.0144	Pb^{2+} = 0.024–0.193	Artificial seawater	[48]
Gold nanoparticles-electroreduced graphene oxide modified SPCE	Plastic	Pb^{2+} = $0.321{\cdot}10^{-3}$	Pb^{2+} = $0–20{\cdot}10^{-3}$	Artificial seawater	[49]
Nafion/ionic liquid/graphene composite modified SPCE	Ceramic	Cd^{2+} = $0.534{\cdot}10^{-3}$ Pb^{2+} = $0.385{\cdot}10^{-3}$	Cd^{2+} = 0.000896–0.896 Pb^{2+} = 0.000483–0.483	Drinking water	[50]
Bismuth/carbon nanotube modified SPCE	Plastic	Cd^{2+} = $6.22{\cdot}10^{-3}$ Pb^{2+} = $6.27{\cdot}10^{-3}$	Cd^{2+} = 0.018–0.896 Pb^{2+} = 0.0096–0.483	River water	[51]
Sputtered gold	Plastic	Cd^{2+} = 0.012 Pb^{2+} = 0.0024	Cd^{2+} = 0–0.445 Pb^{2+} = 0 - 241	Spiked and unspiked river water	[52]
Graphene film modified with chitosan-ferrocene	Plastic	Cd^{2+} = 0.0044 Pb^{2+} = 0.0048	Cd^{2+} = 0.044–3.56 Pb^{2+} = 0.024–0.96	Natural water	[53]
Chromium oxide	Plastic	Cd^{2+} = 0.0267 Pb^{2+} = 0.0144	Cd^{2+} = 0.089–7.12 Pb^{2+} = 0.048–3.86	Industrial wastewater	[54]
Bismuth-polystyrene sulfonate-carbon nanopowder modified SPCE	Ceramic	Cd^{2+} = $1.07{\cdot}10^{-4}$ Pb^{2+} = $1.39{\cdot}10^{-4}$	Cd^{2+} = 0–4 Pb^{2+} = 0–0.217	Mineral and river water	[55]
Graphite ink	Paper	Cd^{2+} = 0.053 Pb^{2+} = 0.034	Cd^{2+} = 0.024–0.483 Pb^{2+} = 0.024–0.483	Spiked acetate saline buffer (pH = 4.5) containing seawater or mud	[56]
Bare SPCE	MNC sheet	Cd^{2+} = 1.01 Pb^{2+} = 0.43	Cd^{2+} = 4.5–14.5 Pb^{2+} = 1.0–10.5	Artificial sweat	This study

SPCE, screen-printed carbon electrode; MNC, microbial nanocellulose; LOD, limit of detection.

CV profiles using ferrocyanide redox probes are common for carbonaceous surfaces due to adsorption effects. The ΔEp and the current peak difference (ΔIp) features combined with Rct decreased for the pre-treated surface, leading to enhanced electrical conductivity, which is desirable for electrochemical sensing devices.

DPV of 17β-estradiol in Fig. 5A and uric acid in Fig. 5C led to linear profiles for the current at the peak *versus* concentration plots in Fig. 5B and 5D, respectively. Linear regressions of the analytical curves for uric acid and estradiol using bare and anodically pre-treated electrodes yielded the following equations: I (A) = 7.9×10^{-10} + 0.008 C_{ua} (M), I

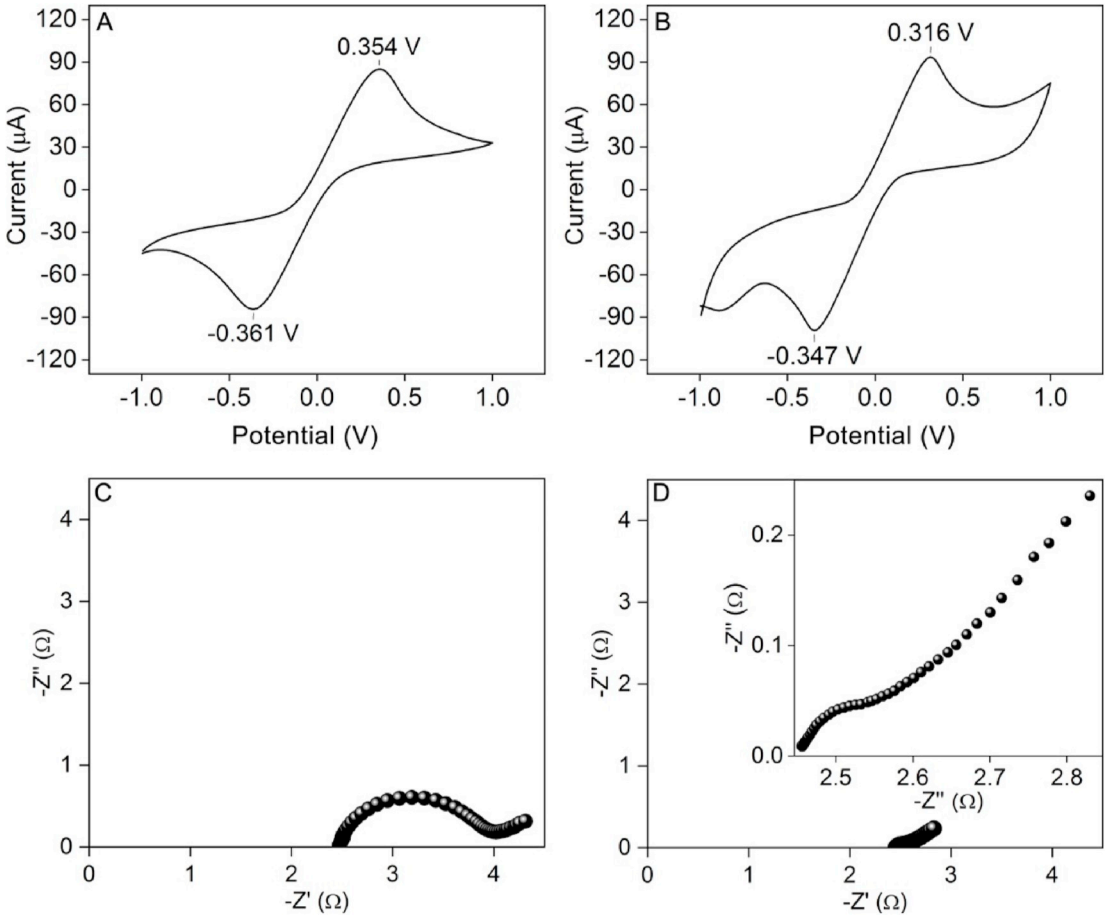

Fig. 4. Cyclic voltammograms for bare (A) and anodically pre-treated (B) electrodes at a scan rate of 50 mV s^{-1}. Complex plane impedance (-Z") spectra (Nyquist diagrams) for bare (C) and anodically pre-treated (D) electrodes. The measurements were performed in 1×10^5 μM PBS solution (pH 7.0) containing 5.0×10^3 μM of redox probe $[Fe(CN)_6]^{4-/3-}$.

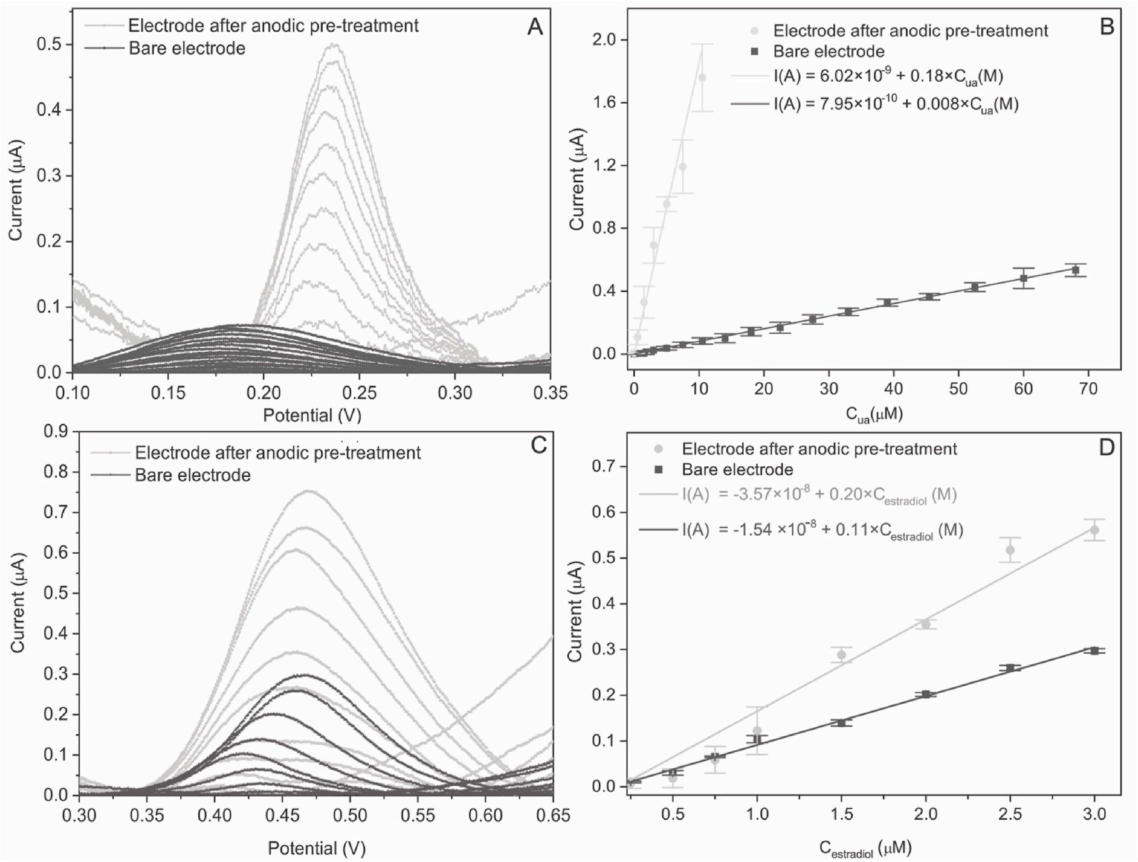

Fig. 5. Differential pulse voltammetry (A and C) and analytical (B and D) curves for detection of 17β-estradiol (top) and uric acid (bottom) in synthetic sweat using bare and anodically pre-treated electrodes. C_{ua} and $C_{estradiol}$ are concentrations of uric acid and 17β-estradiol, respectively.

(A) = 6.0 × 10^{-9} + 0.180 C_{ua} (M), and I (A) = −1.5 × 10^{-8} + 0.10 $C_{estradiol}$ (M), I (A) = −3.6 × 10^{-8} + 0.20 $C_{estradiol}$ (M), with detection limits of 11 and 1.8 μM for uric acid, and 0.27 and 0.58 μM for 17β-estradiol, respectively. Interestingly, anodically pre-treated surfaces exhibited larger electrical conductivity comparing to bare and cathodically pre-treated electrodes (Fig. S4), which reflected in the detection sensitivity 20 times the value for uric acid due to an increase in electrochemically active sites.

Table 2 shows the figures of merit of electrochemical detection of uric acid in relevant biological fluids. Most reports in the literature describe SPCEs on plastic or ceramic substrates. As for detection of uric acid, the LOD in this study is about 13.6 times higher than the uric acid concentration reported in the sweat of a healthy individual [57].

Table 3 shows the figures of merit for electrochemical detection of 17β-estradiol using SPCEs in relevant biological fluids found in the literature. The concentration of 17β-estradiol can span from 0.000004 to 0.011 μM [83] among different age groups, between males and females, and under different conditions (e.g., fertility treatments or use of aromatase inhibitors). Although the limit of detection (0.27 μM) in this work is still orders of magnitude far from clinical significance, a recent work by Muir et al. shows that 17β-estradiol was found in the range of 0.0048–2.6 μM [84,85] in human liquid sweat after stimulated perspiration by using enzyme immunoassays.

3.4. On the reasons why surface pretreatment enhances performance

In order to get further insights on the effect of the pre-treatments on the surface of the SPCEs, we investigated the contact angle between water and the surfaces of bare and electrochemical pre-treated working electrodes. The contact angle of PBS solution varied considerably for bare and anodically pre-treated surfaces, as shown in Fig. 6A and 6B, while the contact angles for the cathodically pre-treated electrode was slightly lower than for the bare electrode (Fig. S5). The latter was hydrophobic with a contact angle of 118° ± 18, which decreased to 62° ± 3 after the anodic surface pre-treatment. The working electrode surface was imaged through SEM to check surface morphology of bare and pre-treated SPCEs, respectively. The electrochemical activation did not seem to affect electrode morphology regardless of the pre-treatment according to the SEM images shown in Fig. 6C and 6D, and Fig. S5B (cathodically pre-treated electrode) or the changes take place over a smaller length scale that is inaccessible to SEM imaging. It is assumed that the pre-treatment leads to a substantial decrease of surface blocking by removal of impurities, such as organic oil, pasting binder or other pollutants on the carbon paste. Additionally, the pre-treatment may expose the original covered graphite and carbon black particles from the carbon paste. As a result, the surface hydrophilicity is significantly improved, which facilitates diffusion of substances to the SPCE surface and contributes to fast electrochemical kinetics/electron transfer rates. A similar trend is observed for SPCEs pre-treated by oxygen- and inert argon-plasma [89,90]. Although there exists an inherent porosity of screen-printed carbon paste on electrodes, the volume of effective pre-treatment is restricted by surface tension of the electrolyte, which in turn may prevent it from getting into small holes.

The activation of bare carbon paste-based SPCE electrodes via pre-treatments has been reported in the literature. For instance, Washe et al. showed an enhancement in electrode performance by soaking the electrode strips in an organic solvent (i.e., N,*N*-dimethylformamide) for etching, followed by drying [91]. Soaking fresh SPCEs into concentrated NaOH (3 × 10^{6} μM) [92] or saturated solution of Na_2CO_3 [93] prior to anodic pre-treatment also improved their electrochemical activity. These pre-treatments were performed on SPCEs printed on plastic or ceramic substrates. Due to the harsh chemical environments

Table 2
Figures of merit for electrochemical detection of uric acid in relevant biological fluids using screen-printed carbon electrodes.

Modification	Substrate	Linear range (μM)	LOD (μM)	Sample	Ref.
Au nanoparticles/Poly (vinyl alcohol) N-methyl-4(4′-formylstyryl)-pyridinium-metho-sulfate-acetal entrapped urate oxidaser	–	–	14	Human sweat	[58]
Nafion	Ceramic	62.5–5000	20.8	UA solution containing 1000 μM ascorbic acid and 1000 μM reduced nicotinamide adenine dinucleotide solution	[59]
Bare SPCE	Ceramic	62.5–5000	2.9	UA solution having 1000 μM ascorbic acid and 1000 μM reduced nicotinamide adenine dinucleotide solution	[59]
Reduced graphene oxide-gold nanocomposite		2.5–1000	0.74	Artificial urine	[60]
Multiwalled carbon nanotube–titanium dioxide nanocomposites	Plastic	30–100	5	PBS solution	[61]
Zinc oxide	Plastic	0.1–169	0.0084	PBS solution	[62]
xanthine oxidase and carbon nanotubes/graphene complexes	–	5–140	2	Human serum	[63]
Zinc oxide/graphene	Ceramic	1–100	0.43	Spiked urine	[64]
Reduced graphene oxide and gold nanoparticles	–	25–200	5.4	Artificial and human urine	[65]
Nafion/gold nanoparticles	Ceramic	0.5–600	0.25	Blood human serum	[66]
Reduced graphene oxide paste on F-doped tin oxide	Ceramic	5–300	0.39	Spiked urine	[67]
single walled carbon nanotubes dispersed in 1 butyl-3-metilimidazolium tetrafluorborate and chitosan	Ceramic	0.50–1000	0.17	Human urine	[68]
Prussian blue/poly(4-aminosalicylic acid)/Uricase	Ceramic	10–200	3	Urine	[69]
Graphene oxide/iron oxide-silica core-shell nanocomposite	Ceramic	0.75–300	0.57	Human urine	[69]
Graphene oxide nanoribbons and poly(3,4-ethylenedioxythiophene):polystyrene sulfonate	–	0.05–16.55	0.011	PBS solution containing ascorbic acid and dopamine	[70]
β-cyclodextrin/reduced graphene oxide	–	0.08–150	0.026	Human blood serum	[71]
Bare carbon screen-printed electrode	Paper	0 - 2000	80	Human urine	[72]
Reduced graphene oxide	Plastic	10- 3000	0.1	Human urine (spiked)	[73]
Silver nanowire/reduced graphene oxide	Plastic	35–300	0.30	PBS solution containing dopamine and ascorbic acid	[74]
Multiwall carbon nanotubes	Ceramic	1–100	0.86	Human urine	[75]
Prussian blue/uricase	Plastic	30–300	10	Human blood serum	[76]
Cobalt phthalocyanine/uricase	Plastic	15–250	15	Urine	[77]
Reduce graphene oxide	Plastic	0.8–2500	0.20	Human urine	[78]
Multi-wall carbon nanotubes	Plastic	0–30	0.458	PBS solution	[79]
Pre-anodized nontronite clay	Plastic	2–40	0.42	Human urine	[80]
Uricase/cobalt phthalocyanine/cellulose acetate	–	13-1000	13	Glycine buffer	[81]
Ascorbate oxidase	Plastic	5–151	2.54	PBS solution	[82]
Bare SPCE after anodic treatment	MNC sheet	0–70	1.8	PBS solution	This study

SPCE, screen-printed carbon electrode; MNC, microbial nanocellulose; LOD, limit of detection; PBS, phosphate-buffered saline; UA, uric acid.

(e.g. strong alkaline solutions or use of carcinogenic solvents) such pre-treatments could place an irreversible deleterious effect on biopolymeric substrates such as MNC, being incompatible with biological purposes. Nevertheless, Kostaki et al. showed that SPCE pre-treated with an aqueous solution of H_2SO_4 1×10^5 μM (i.e., same concentration used in this work) under anodic galvanostatic conditions can enhance the electrochemical performance of untreated SPCEs. However, the pre-treatment is 6 times longer than in our study. Other activation procedures (e.g., based on heat [94], UV/ozone [95], UV laser [96], oxygen- [89], and argon-plasma [90] have been shown to enhance the electron-transfer rates at SPCE, but may not be compatible with their single-use field operation or not suitable for mass production [97].

The analysis with energy-dispersive X-ray (EDX) spectroscopy for a working electrode in Fig. S6 points to an increase in oxygen content of the anodically pre-treated SPCE compared to the bare electrode. The XPS survey spectra to determine the elemental compositions of the samples are presented in Fig. S7, A-D. Fig. 7 shows the high-resolution spectra of O1s and C1s for pure MNC sheet surface (substrate; O1s/C1s atomic ratio: 0.53 ± 0.08), typical of cellulose [98], which are remarkably different from those of bare or pre-treated SPCE tracks. The survey spectra in Fig. 7 indicate that the anodic pre-treatment increased oxygen contents from 4.4 ± 0.8 at.% (O1s/C1s ratio: 0.05 ± 0.02, bare electrode) to 7.9 ± 0.8 at.% (O1s/C1s ratio: 0.10 ± 0.01). This is consistent with the increased current density and decreased charge-transfer resistance due to the increased oxygen content on electrode surface and the coexistence of reactive and hydrocarbon groups. The deconvolution of the broad C1s peaks in the survey spectra points to four major types of carbon: 284.0 and 284.8–284.9 eV, characteristic of aliphatic carbons (sp^2 and sp^3, respectively); 86.0 eV, assigned to carbon atoms saturatedly bonded to single oxygen atoms, e.g., hydroxyl

Table 3
Figures of merit for electrochemical detection of 17β-estradiol in relevant biological fluids using screen-printed carbon electrodes.

Modification	Substrate	Linear range (μM)	LOD (μM)	Sample	Ref.
Immunosensor rabbit anti-mouse IgG and 17β-estradiol monoclonal mouse antibody (anti-E2)	Plastic	0.000092–0.00183	0.000184	Serum	[86]
Anti-estradiol-Biotin	Ceramic	0.0000037–0.000918	0.0000028	Certified serum Spike human urine	[87]
Multi-walled carbon nanotubes/thionine/gold nanoparticles/17β-estradiol monoclonal antibody	Paper	0.000000037–0.00037	0.000037	PBS solution	[88]
Bare carbon screen-printed electrode after anodic treatment	MNC sheet	0–3	0.27	PBS solution	This study

LOD, limit of detection; MNC, microbial nanocellulose; PBS, phosphate-buffered saline.

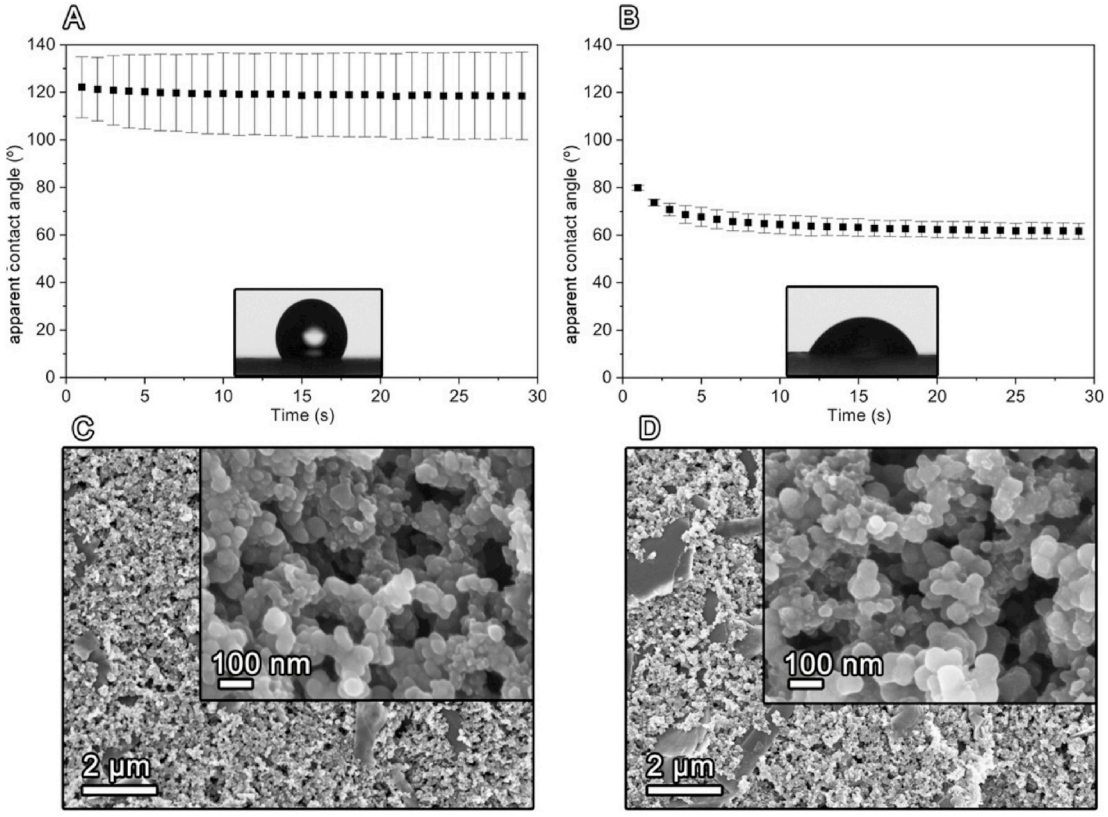

Fig. 6. Picture of a PBS aqueous solution drop on (top) and scanning electron microscopy (SEM) images (bottom) of the surfaces of bare (A and C) and anodically (B and D) pre-treated working electrodes. The inset of panels C and D present magnified SEM images.

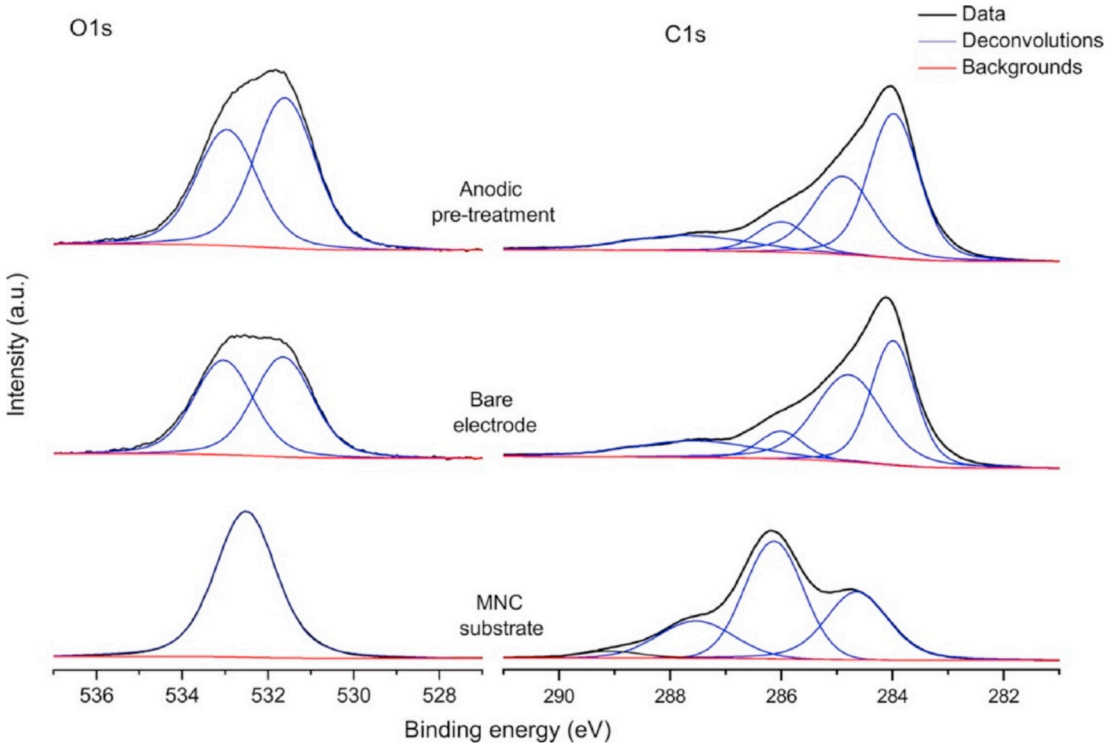

Fig. 7. High-resolution X-ray photoelectron spectra of O1s and C1s of bare and anodically pre-treated electrodes as well as of the microbial nanocellulose (MNC) substrate.

groups; and 287.6–287.7 eV, attributed to carbon atoms unsaturatedly bonded to single oxygen atoms, e.g., carbonyl groups [98–100]. Indeed, the pre-treatments decreased the content of unoxidized sp^3 carbons (40.9 – bare – to 31.4 at.%– anodic) – while they increased the unsaturated oxidized carbons, e.g., –C–O– (8.5–9.8 at.%, respectively). Conversely, aliphatic sp^2 was increased (34.6 – bare – to 46.7 at.%–

anodic) at the expense of decreased saturated oxidized carbons (8.5–9.8 at.%, respectively). This trend is confirmed in the deconvolution of the O1s peak, which shows two types of oxygen atoms in all electrodes subjected to anodic pre-treatment: 531.6 and 532.9–533.0 eV, assigned to organic –C–O– and –C═O groups. While the former was increased upon pre-treatment (52.3 – bare – to 56.4 at. % – anodic), the latter was decreased (47.7–43.6 at.%). A similar behavior is observed for electrodes after cathodic pre-treatment (Figure S7, E and F) The increased oxygen contents on the electrode surface induced by the pre-treatments is consistent with the reported removal of surface contaminants and formation of increasing density of oxygen-containing groups in pre-treated carbon electrodes (such as quinoidal, phenolic, and carboxyl functionalities) [93,97,101].

A more detailed analysis using Kelvin Probe Force Microscopy (KPFM) was conducted to correlate the increase in sensitivity and the local electric properties of SPCEs after pre-treatment. Changes on the electrical properties of electrode surfaces can be assessed by measuring the gradient capacitance (∂C/∂z) between a conducting atomic force microscopy (AFM) cantilever tip and the working electrode surface. These measurements are carried out by applying an AC voltage to the tip and monitoring its response at the AC frequency, thereby mapping the work function (or surface potential) of the sample with high spatial resolution. Fig. 8 shows topographical AFM and KPFM images of bare and pre-treated electrodes. Bare electrodes showed an average ∂C/∂z average of 1.58 a. u. After cathodic and anodic pre-treatments, the average ∂C/∂z increased to 1.96 (Fig. S5D) and 2.30 a. u, respectively. It is suggested that the increase of sensitivity of SPCE pre-treated with anodic treatment may be related to the increase of local gradient capacitance when compared to bare. As observed in CV and EIS measurements, the oxygenated functional groups increased the electrical conductivity on the carbon surface.

4. Conclusion

We have explored the versatility of a sensing platform made with screen-printed carbon electrodes on nanocellulose to detect biologically relevant target species such as toxic metals (e.g., cadmium and lead), uric acid, and 17β-estradiol in artificial sweat. The electrochemical features were improved in terms of electrical conductivity using anodic pre-treatment in diluted sulfuric acid, leading to faster electron transfer rate, lower limit of detection, and improved sensitivity compared with as-prepared surfaces. In addition to these favorable analytical features, the sensing platform obtained with MNCs may solve the adhesion problem, thus allowing skin integration in wearable devices. Indeed, some of the important limitations of current clinical monitoring tools, related to cumbersome wiring, rigid packing with brittle components,

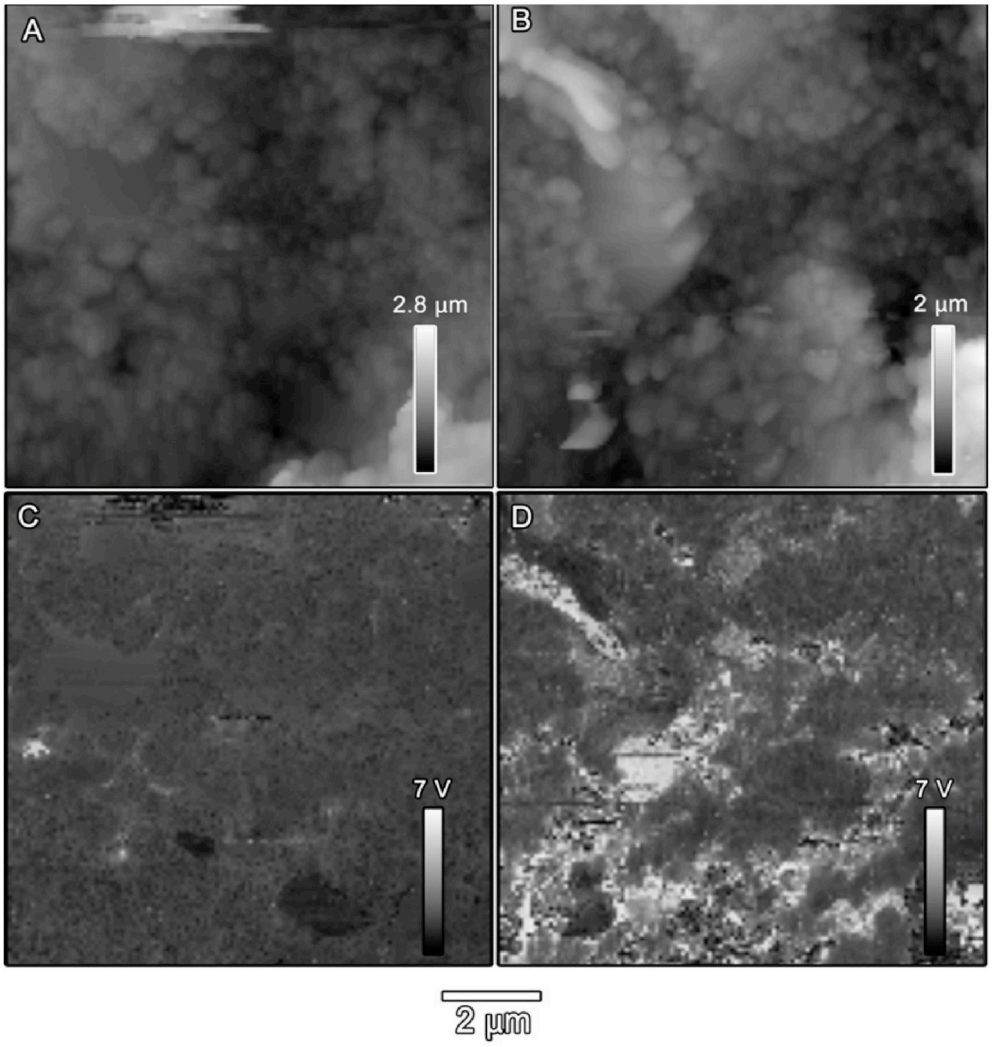

Fig. 8. Topographic atomic force microscopy (top) and Kelvin probe force microscopy (∂C/∂z; bottom) images of as-prepared (A, C) and anodically (B, D) pre-treated electrodes.

and bulk devices that require straps or adhesive tapes for mounting on the skin [12,102], can be addressed with the methodology presented here.

Furthermore, a number of new developments may be pursued in the near future. One may focus on optimizing conductive inks for carbonaceous electrode materials to employ in immunosensors, and even combine drug delivery therapies in theranostic strategies. Other methodologies will have to be used to overcome the limitation in our work in which sufficient electrolyte fluid (sweat) must be in contact with the sensor for the amperometric signal generation (in situ analyses). One may, for example, design microfluidics in MNC sheets for sweat collection, storage for ideal quantitative analyses to provide the adequate sweat amount/sweat rate. Another possibility would be to obtain electric circuits built-in bacterial cellulose membranes for fully flexible skin-mounted and real-time analysis, and introduce a conformal electronic interface that provides wireless data transmission. With regard to multiple sensing purposes, MNCs may be used to integrate sensing of sweat pH and temperature, and employ sweat release stimulators (ionofers/agonist agent or voltage-induced sweat release stimulation/iontophoresis electrodes).

Credit author statement

Robson Rosa da Silva: Conceptualization, Investigation, Methodology, Writing-Original draft preparation, Writing - review & editing, Project administration, Funding acquisition. 'Paulo Augusto Raymundo-Pereira: Methodology, Validation, Investigation, Visualization, Formal analysis, Writing - review & editing Anderson Massahiro de Campos: Investigation, Validation. Deivy Wilson Masso: Conceptualization, Investigation, Methodology. Caio Gomide Otoni:: Resources, Writing - review & editing. Hernane da Silva Barud: Resources, Writing - review & editing. Carlos Alberto Rodrigues Costa: Resources, Writing - review & editing. Rafael Romano Domeneguetti: Resources, Writing - review & editing. Debora T. Balogh: Resources, Writing - review & editing. Sidney J. L. Ribeiro: Resources, Supervision. Osvaldo N. Oliveira: Resources, Supervision, Writing - review & editing.

Declaration of competing interest

The authors declare no competing financial interest.

Acknowledgments

The authors are thankful to FAPESP (2016/06612–6, 2016/01919–6, 2015/01770–0, 2013/14262–7), CNPq (423952/2018-8), and CAPES for the financial support. Brazilian Nanotechnology National Laboratory (LNNano), CNPEM/MCTIC, is acknowledged for AFM and XPS runs.

Appendix A. Supplementary data

Supplementary data to this article can be found online at https://doi.org/10.1016/j.talanta.2020.121153.

References

[1] P. Düking, A. Hotho, H.-C. Holmberg, F.K. Fuss, B. Sperlich, Comparison of non-invasive individual monitoring of the training and health of athletes with commercially available wearable technologies, Front. Physiol. 7 (2016), https://doi.org/10.3389/fphys.2016.00071.

[2] W. Gao, S. Emaminejad, H.Y.Y. Nyein, S. Challa, K. Chen, A. Peck, H.M. Fahad, H. Ota, H. Shiraki, D. Kiriya, D.-H. Lien, G.A. Brooks, R.W. Davis, A. Javey, Fully integrated wearable sensor arrays for multiplexed in situ perspiration analysis, Nature 529 (2016) 509–514, https://doi.org/10.1038/nature16521.

[3] Z. Sonner, E. Wilder, J. Heikenfeld, G. Kasting, F. Beyette, D. Swaile, F. Sherman, J. Joyce, J. Hagen, N. Kelley-Loughnane, R. Naik, The microfluidics of the eccrine sweat gland, including biomarker partitioning, transport, and biosensing implications, Biomicrofluidics 9 (2015) 031301, , https://doi.org/10.1063/1.4921039.

[4] Y.J. Hong, H. Lee, J. Kim, M. Lee, H.J. Choi, T. Hyeon, D.-H. Kim, Multifunctional wearable system that integrates sweat-based sensing and vital-sign monitoring to estimate pre-/post-exercise glucose levels, Adv. Funct. Mater. 28 (2018) 1805754, https://doi.org/10.1002/adfm.201805754.

[5] M. Parrilla, M. Cuartero, G.A. Crespo, Wearable potentiometric ion sensors, TrAC Trends Anal. Chem. (Reference Ed.) 110 (2019) 303–320, https://doi.org/10.1016/j.trac.2018.11.024.

[6] D.B. Speedy, T.D. Noakes, C. Schneider, Exercise-associated hyponatremia: a review, Emerg. Med. 13 (2001) 17–27, https://doi.org/10.1046/j.1442-2026.2001.00173.x.

[7] J. Zhao, Y. Lin, J. Wu, H.Y.Y. Nyein, M. Bariya, L.-C. Tai, M. Chao, W. Ji, G. Zhang, Z. Fan, A. Javey, A fully integrated and self-powered smartwatch for continuous sweat glucose monitoring, ACS Sens. (2019) 9b00891, , https://doi.org/10.1021/acssensors.9b00891 acssensors.

[8] N. De Giovanni, N. Fucci, The current status of sweat testing for drugs of abuse: a review, Curr. Med. Chem. 20 (2013) 545–561, https://doi.org/10.2174/092986713804910139.

[9] L.E. Gibson, R.E. Cooke, A test for concentration of electrolytes in sweat in cystic fibrosis of the pancreas utilizing pilocarpine by iontophoresis, Pediatrics 23 (1959) 545–549.

[10] W. Jia, A.J. Bandodkar, G. Valdés-Ramírez, J.R. Windmiller, Z. Yang, J. Ramírez, G. Chan, J. Wang, Electrochemical tattoo biosensors for real-time noninvasive lactate monitoring in human perspiration, Anal. Chem. 85 (2013) 6553–6560, https://doi.org/10.1021/ac401573r.

[11] J. Choi, A.J. Bandodkar, J.T. Reeder, T.R. Ray, A. Turnquist, S.B. Kim, N. Nyberg, A. Hourlier-Fargette, J.B. Model, A.J. Aranyosi, S. Xu, R. Ghaffari, J.A. Rogers, Soft, skin-integrated multifunctional microfluidic systems for accurate colorimetric analysis of sweat biomarkers and temperature, ACS Sens. 4 (2019) 379–388, https://doi.org/10.1021/acssensors.8b01218.

[12] M. Bariya, H.Y.Y. Nyein, A. Javey, Wearable sweat sensors, Nat. Electron. 1 (2018) 160–171, https://doi.org/10.1038/s41928-018-0043-y.

[13] M. Bariya, Z. Shahpar, H. Park, J. Sun, Y. Jung, W. Gao, H.Y.Y. Nyein, T.S. Liaw, L.-C. Tai, Q.P. Ngo, M. Chao, Y. Zhao, M. Hettick, G. Cho, A. Javey, Roll-to-Roll gravure printed electrochemical sensors for wearable and medical devices, ACS Nano 12 (2018) 6978–6987, https://doi.org/10.1021/acsnano.8b02505.

[14] A.J. Bandodkar, D. Molinnus, O. Mirza, T. Guinovart, J.R. Windmiller, G. Valdés-Ramírez, F.J. Andrade, M.J. Schöning, J. Wang, Epidermal tattoo potentiometric sodium sensors with wireless signal transduction for continuous non-invasive sweat monitoring, Biosens. Bioelectron. 54 (2014) 603–609, https://doi.org/10.1016/j.bios.2013.11.039.

[15] J. Choi, R. Ghaffari, L.B. Baker, J.A. Rogers, Skin-interfaced systems for sweat collection and analytics, Sci. Adv. 4 (2018) eaar3921, https://doi.org/10.1126/sciadv.aar3921.

[16] K. Godbey, Wearable Sensors – from the "Skin-Side" Out, Saint Paul, 2016, http://multimedia.3m.com/mws/media/980466O/wearable-sensor-white-paper.pdf?elqTrackId=8f1761bb99754d0aabf710e4a0bff819&elqaid=1449&elqat=2.

[17] I. Hwang, H.N. Kim, M. Seong, S.-H. Lee, M. Kang, H. Yi, W.G. Bae, M.K. Kwak, H.E. Jeong, Multifunctional smart skin adhesive patches for advanced health care, Adv. Healthc. Mater. 7 (2018) 1800275, https://doi.org/10.1002/adhm.201800275.

[18] C. Moulherat, M. Tengberg, J.-F. Haquet, B. Mille, First evidence of cotton at neolithic mehrgarh, Pakistan: analysis of mineralized fibres from a copper bead, J. Archaeol. Sci. 29 (2002) 1393–1401, https://doi.org/10.1006/jasc.2001.0779.

[19] A. Ferrer, E. Quintana, I. Filpponen, I. Solala, T. Vidal, A. Rodríguez, J. Laine, O.J. Rojas, Effect of residual lignin and heteropolysaccharides in nanofibrillar cellulose and nanopaper from wood fibers, Cellulose 19 (2012) 2179–2193, https://doi.org/10.1007/s10570-012-9788-z.

[20] H.G. de Oliveira Barud, R.R. da Silva, H. da Silva Barud, A. Tercjak, J. Gutierrez, W.R. Lustri, O.B. de Oliveira, S.J.L. Ribeiro, A multipurpose natural and renewable polymer in medical applications: bacterial cellulose, Carbohydr. Polym. 153 (2016) 406–420, https://doi.org/10.1016/j.carbpol.2016.07.059.

[21] G. Pacheco, C.V. de Mello, B.G. Chiari-Andréo, V.L.B. Isaac, S.J.L. Ribeiro, É. Pecoraro, E. Trovatti, Bacterial cellulose skin masks-Properties and sensory tests, J. Cosmet. Dermatol. 17 (2018) 840–847, https://doi.org/10.1111/jocd.12441.

[22] M.E.S. Piadozo, M. Gama, F. Dourado, S. Bielecki (Eds.), Nata de Coco Industry in the Philippines, Bact. Nanocellulose, Elsevier, Amsterdan, 2016, pp. 215–229, , https://doi.org/10.1016/B978-0-444-63458-0.00013-5.

[23] M. Phisalaphong, T.K. Tran, S. Taokaew, R. Budiraharjo, G.G. Febriana, D.N. Nguyen, S. Chu-Ky, F. Dourado, Nata de coco Industry in Vietnam, Thailand, and Indonesia, in: M. Gama, F. Dourado, S. Bielecki (Eds.), Bact. Nanocellulose from Biotechnol. To Bio-Economy, first ed., Elsevier, Amsterdan, 2016, pp. 231–236, , https://doi.org/10.1016/B978-0-444-63458-0.00014-7.

[24] D. Klemm, E.D. Cranston, D. Fischer, M. Gama, S.A. Kedzior, D. Kralisch, F. Kramer, T. Kondo, T. Lindström, S. Nietzsche, K. Petzold-Welcke, F. Rauchfuß, Nanocellulose as a natural source for groundbreaking applications in materials science: today's state, Mater. Today 21 (2018) 720–748, https://doi.org/10.1016/j.mattod.2018.02.001.

[25] J.D. Fontana, A.M. De Souza, C.K. Fontana, I.L. Torriani, J.C. Moreschi, B.J. Gallotti, S.J. De Souza, G.P. Narcisco, J.A. Bichara, L.F.X. Farah, Acetobacter cellulose pellicle as a temporary skin substitute, Appl. Biochem. Biotechnol. 24–25 (1990) 253–264, https://doi.org/10.1007/BF02920250.

[26] R. Portela, C.R. Leal, P.L. Almeida, R.G. Sobral, Bacterial cellulose: a versatile biopolymer for wound dressing applications, Microb. Biotechnol. 12 (2019) 586–610, https://doi.org/10.1111/1751-7915.13392.

[27] L. Fu, J. Zhang, G. Yang, Present status and applications of bacterial cellulose-based materials for skin tissue repair, Carbohydr. Polym. 92 (2013) 1432–1442, https://doi.org/10.1016/j.carbpol.2012.10.071.
[28] L.C. Tomé, L. Brandão, A.M. Mendes, A.J.D. Silvestre, C.P. Neto, A. Gandini, C.S.R. Freire, I.M. Marrucho, Preparation and characterization of bacterial cellulose membranes with tailored surface and barrier properties, Cellulose 17 (2010) 1203–1211, https://doi.org/10.1007/s10570-010-9457-z.
[29] E. Morales-Narváez, H. Golmohammadi, T. Naghdi, H. Yousefi, U. Kostiv, D. Horák, N. Pourreza, A. Merkoçi, Nanopaper as an optical sensing platform, ACS Nano 9 (2015) 7296–7305, https://doi.org/10.1021/acsnano.5b03097.
[30] S. Abbasi-Moayed, H. Golmohammadi, A. Bigdeli, M.R. Hormozi-Nezhad, A rainbow ratiometric fluorescent sensor array on bacterial nanocellulose for visual discrimination of biothiols, Analyst 143 (2018) 3415–3424, https://doi.org/10.1039/C8AN00637G.
[31] E. Zor, S. Alpaydin, A. Arici, M.E. Saglam, H. Bingol, Photoluminescent nanopaper-based microcuvette for iodide detection in seawater, Sensor. Actuator. B Chem. 254 (2018) 1216–1224, https://doi.org/10.1016/j.snb.2017.07.208.
[32] B. Zhang, J. Zhou, S. Li, X. Zhang, D. Huang, Y. He, M. Wang, G. Yang, Y. Shen, Hydrogen peroxide biosensor based on microperoxidase-11 immobilized on flexible MWCNTs-BC nanocomposite film, Talanta 131 (2015) 243–248, https://doi.org/10.1016/j.talanta.2014.07.027.
[33] T. Zhang, W. Wang, D. Zhang, X. Zhang, Y. Ma, Y. Zhou, L. Qi, Biotemplated synthesis of gold nanoparticle-bacteria cellulose nanofiber nanocomposites and their application in biosensing, Adv. Funct. Mater. 20 (2010) 1152–1160, https://doi.org/10.1002/adfm.200902104.
[34] N. Cheeveewattanagul, E. Morales-Narváez, A.-R.H.A. Hassan, J.F. Bergua, W. Surareungchai, M. Somasundrum, A. Merkoçi, Straightforward immunosensing platform based on graphene oxide-decorated nanopaper: a highly sensitive and fast biosensing approach, Adv. Funct. Mater. 27 (2017) 1702741, https://doi.org/10.1002/adfm.201702741.
[35] J.G. Barajas-Carmona, L. Francisco-Aldana, E. Morales-Narváez, Wearable nanoplasmonic patch detecting sun/UV exposure, Anal. Chem. 89 (2017) 13589–13595, https://doi.org/10.1021/acs.analchem.7b04066.
[36] R. Mangayil, S. Rajala, A. Pammo, E. Sarlin, J. Luo, V. Santala, M. Karp, S. Tuukkanen, Engineering and characterization of bacterial nanocellulose films as low cost and flexible sensor material, ACS Appl. Mater. Interfaces 9 (2017), https://doi.org/10.1021/acsami.7b04927 19048–19056.
[37] W.J. Paschoalino, S. Kogikoski, J.T.C. Barragan, J.F. Giarola, L. Cantelli, T.M. Rabelo, T.M. Pessanha, L.T. Kubota, Emerging considerations for the future development of electrochemical paper-based analytical devices, ChemElectroChem 6 (2019) 10–30, https://doi.org/10.1002/celc.201800677.
[38] G. Ibáñez-Redín, R.H.M. Furuta, D. Wilson, F.M. Shimizu, E.M. Materon, L.M.R.B. Arantes, M.E. Melendez, A.L. Carvalho, R.M. Reis, M.N. Chaur, D. Gonçalves, O.N. Oliveira Jr., Screen-printed interdigitated electrodes modified with nanostructured carbon nano-onion films for detecting the cancer biomarker CA19-9, Mater. Sci. Eng. C 99 (2019) 1502–1508, https://doi.org/10.1016/j.msec.2019.02.065.
[39] D. Wilson, E.M. Materón, G. Ibáñez-Redín, R.C. Faria, D.S. Correa, O.N. Oliveira, Electrical detection of pathogenic bacteria in food samples using information visualization methods with a sensor based on magnetic nanoparticles functionalized with antimicrobial peptides, Talanta 194 (2019) 611–618, https://doi.org/10.1016/j.talanta.2018.10.089.
[40] A.M. Campos, P.A. Raymundo-Pereira, C.D. Mendonça, M.L. Calegaro, S.A.S. Machado, O.N. Oliveira, Size control of carbon spherical shells for sensitive detection of paracetamol in sweat, saliva, and urine, ACS Appl. Nano Mater. 1 (2018) 654–661, https://doi.org/10.1021/acsanm.7b00139.
[41] J.N. Miller, Basic statistical methods for Analytical Chemistry. Part 2. Calibration and regression methods. A review, Analyst 116 (1991) 3, https://doi.org/10.1039/an9911600003.
[42] J.C. Miller, J.N. Miller, Basic statistical methods for analytical chemistry. Part I. Statistics of repeated measurements. A review, Analyst 113 (1988) 1351, https://doi.org/10.1039/an9881301351.
[43] M.E. Sears, K.J. Kerr, R.I. Bray, Arsenic, cadmium, lead, and mercury in sweat: a systematic review, J. Environ. Public Health (2012) 1–10, https://doi.org/10.1155/2012/184745 2012.
[44] W. Gao, H.Y.Y. Nyein, Z. Shahpar, H.M. Fahad, K. Chen, S. Emaminejad, Y. Gao, L.-C. Tai, H. Ota, E. Wu, J. Bullock, Y. Zeng, D.-H. Lien, A. Javey, Wearable microsensor array for multiplexed heavy metal monitoring of body fluids, ACS Sens. 1 (2016) 866–874, https://doi.org/10.1021/acssensors.6b00287.
[45] J.R. Cohn, E.A. Emmett, The excretion of trace metals in human sweat, Toxicol. Occup. Med, Elsevier, 1979, pp. 319–328, , https://doi.org/10.1016/B978-0-444-00288-4.50036-0.
[46] V. Mudgal, N. Madaan, A. Mudgal, R.B. Singh, S. Mishra, Effect of toxic metals on human health, Open Nutraceuticals J. 3 (2010) 94–99, https://doi.org/10.2174/1876396001003010094.
[47] P. Sundaresan, Electrochemical activation of screen printed carbon electrode for the determination of antibiotic drug metronidazole, Int. J. Electrochem. Sci. (2018) 1441–1451, https://doi.org/10.20964/2018.02.05.
[48] G. Aragay, J. Pons, A. Merkoçi, Enhanced electrochemical detection of heavy metals at heated graphite nanoparticle-based screen-printed electrodes, J. Mater. Chem. 21 (2011) 4326, https://doi.org/10.1039/c0jm03751f.
[49] B. Molinero-Abad, D. Izquierdo, L. Pérez, I. Escudero, M.J. Arcos-Martínez, Comparison of backing materials of screen printed electrochemical sensors for direct determination of the sub-nanomolar concentration of lead in seawater, Talanta 182 (2018) 549–557, https://doi.org/10.1016/j.talanta.2018.02.005.
[50] S. Chaiyo, E. Mehmeti, K. Žagar, W. Siangproh, O. Chailapakul, K. Kalcher, Electrochemical sensors for the simultaneous determination of zinc, cadmium and lead using a Nafion/ionic liquid/graphene composite modified screen-printed carbon electrode, Anal. Chim. Acta 918 (2016) 26–34, https://doi.org/10.1016/j.aca.2016.03.026.
[51] G. Hwang, W. Han, J. Park, S. Kang, Determination of trace metals by anodic stripping voltammetry using a bismuth-modified carbon nanotube electrode, Talanta 76 (2008) 301–308, https://doi.org/10.1016/j.talanta.2008.02.039.
[52] S. Laschi, I. Palchetti, M. Mascini, Gold-based screen-printed sensor for detection of trace lead, Sensor. Actuator. B Chem. 114 (2006) 460–465, https://doi.org/10.1016/j.snb.2005.05.028.
[53] S. Liu, T. Wu, F. Li, Q. Zhang, X. Dong, L. Niu, Disposable graphene sensor with an internal reference electrode for stripping analysis of heavy metals, Anal. Methods. 10 (2018), https://doi.org/10.1039/C8AY00221E 1986–1992.
[54] Z. Koudelkova, T. Syrovy, P. Ambrozova, Z. Moravec, L. Kubac, D. Hynek, L. Richtera, V. Adam, Determination of zinc, cadmium, lead, copper and silver using a carbon paste electrode and a screen printed electrode modified with chromium(III) oxide, Sensors 17 (2017) 1832, https://doi.org/10.3390/s17081832.
[55] R. María-Hormigos, M.J. Gismera, J.R. Procopio, M.T. Sevilla, Disposable screen-printed electrode modified with bismuth–PSS composites as high sensitive sensor for cadmium and lead determination, J. Electroanal. Chem. 767 (2016) 114–122, https://doi.org/10.1016/j.jelechem.2016.02.025.
[56] M. Medina-Sánchez, M. Cadevall, J. Ros, A. Merkoçi, Eco-friendly electrochemical lab-on-paper for heavy metal detection, Anal. Bioanal. Chem. 407 (2015) 8445–8449, https://doi.org/10.1007/s00216-015-9022-6.
[57] C.-T. Huang, M.-L. Chen, L.-L. Huang, I.-F. Mao, Uric acid and urea in human sweat, Chin. J. Physiol. 45 (2002) 109–115 http://www.cps.org.tw/issues/file/18f74fb8b703541ebdde71c9aad5ce31.pdf.
[58] S. RoyChoudhury, Y. Umasankar, S. Bhansali, A wearable electrochemical sensor to monitor progression of wound healing, ECS Trans 80 (2017) 1345–1353, https://doi.org/10.1149/08010.1345ecst.
[59] Z. Xu, M. Zhang, H. Zou, J. Liu, D. Wang, J. Wang, L. Wang, Non-enzymatic electrochemical detection of uric acid with electrodeposited Nafion film, J. Electroanal. Chem. 841 (2019) 129–134, https://doi.org/10.1016/j.jelechem.2019.04.028.
[60] K. Income, N. Ratnarathorn, N. Khamchaiyo, C. Srisuvo, L. Ruckthong, W. Dungchai, Disposable nonenzymatic uric acid and creatinine sensors using μPAD coupled with screen-printed reduced graphene oxide-gold nanocomposites, Int. J. Anal. Chem. (2019) 1–11, https://doi.org/10.1155/2019/3457247 2019.
[61] A. Aoboun, B. Cherdhirunkorn, C. Pechyen, Development of screen printed electrode using MWCNTs–TiO2 nanocomposite as a low-cost device for uric acid detection in urine, J. Mater. Sci. Mater. Electron. 30 (2019) 2403–2412, https://doi.org/10.1007/s10854-018-0513-z.
[62] S. Kogularasu, M. Akilarasan, S.-M. Chen, T.-W. Chen, B.-S. Lou, Urea-based morphological engineering of ZnO; for the biosensing enhancement towards dopamine and uric acid in food and biological samples, Mater. Chem. Phys. 227 (2019) 5–11, https://doi.org/10.1016/j.matchemphys.2019.01.041.
[63] Y. Si, J.W. Park, S. Jung, G.-S. Hwang, E. Goh, H.J. Lee, Layer-by-layer electrochemical biosensors configuring xanthine oxidase and carbon nanotubes/graphene complexes for hypoxanthine and uric acid in human serum solutions, Biosens. Bioelectron. 121 (2018) 265–271, https://doi.org/10.1016/j.bios.2018.08.074.
[64] R. Rezaei, M.M. Foroughi, H. Beitollahi, R. Alizadeh, Electrochemical sensing of uric acid using a ZnO/graphene nanocomposite modified graphite screen printed electrode, Russ. J. Electrochem. 54 (2018) 860–866, https://doi.org/10.1134/S1023193518130347.
[65] D. Ji, Z. Liu, L. Liu, S.S. Low, Y. Lu, X. Yu, L. Zhu, C. Li, Q. Liu, Smartphone-based integrated voltammetry system for simultaneous detection of ascorbic acid, dopamine, and uric acid with graphene and gold nanoparticles modified screen-printed electrodes, Biosens. Bioelectron. 119 (2018) 55–62, https://doi.org/10.1016/j.bios.2018.07.074.
[66] N. Stozhko, M. Bukharinova, L. Galperin, K. Brainina, A nanostructured sensor based on gold nanoparticles and nafion for determination of uric acid, Biosensors 8 (2018) 21, https://doi.org/10.3390/bios8010021.
[67] A.J.S. Ahammad, T. Islam, M.M. Hasan, M.N.I. Mozumder, R. Karim, N. Odhikari, P.R. Pal, S. Sarker, D.M. Kim, Reduced graphene oxide screen-printed FTO as highly sensitive electrodes for simultaneous determination of dopamine and uric acid, J. Electrochem. Soc. 165 (2018) B174–B183, https://doi.org/10.1149/2.0121805jes.
[68] E. Nagles, O. García-Beltrán, J.A. Calderón, Evaluation of the usefulness of a novel electrochemical sensor in detecting uric acid and dopamine in the presence of ascorbic acid using a screen-printed carbon electrode modified with single walled carbon nanotubes and ionic liquids, Electrochim. Acta 258 (2017) 512–523, https://doi.org/10.1016/j.electacta.2017.11.093.
[69] F.S. da Cruz, F. de S. Paula, D.L. Franco, W.T.P. dos Santos, L.F. Ferreira, Electrochemical detection of uric acid using graphite screen-printed electrodes modified with Prussian blue/poly(4-aminosalicylic acid)/Uricase, J. Electroanal. Chem. 806 (2017) 172–179, https://doi.org/10.1016/j.jelechem.2017.10.070.
[70] C.-H. Su, C.-L. Sun, Y.-C. Liao, Printed combinatorial sensors for simultaneous detection of ascorbic acid, uric acid, dopamine, and nitrite, ACS Omega 2 (2017) 4245–4252, https://doi.org/10.1021/acsomega.7b00681.
[71] Q. Qin, X. Bai, Z. Hua, Electropolymerization of a conductive β-cyclodextrin polymer on reduced graphene oxide modified screen-printed electrode for simultaneous determination of ascorbic acid, dopamine and uric acid, J. Electroanal. Chem. 782 (2016) 50–58, https://doi.org/10.1016/j.jelechem.2016.10.004.

[72] Y. Yao, C. Zhang, A novel screen-printed microfluidic paper-based electrochemical device for detection of glucose and uric acid in urine, Biomed. Microdevices 18 (2016) 92, https://doi.org/10.1007/s10544-016-0115-6.
[73] P. Kanyong, S. Rawlinson, J. Davis, A voltammetric sensor based on chemically reduced graphene oxide-modified screen-printed carbon electrode for the simultaneous analysis of uric acid, ascorbic acid and dopamine, Chemosensors 4 (2016) 25, https://doi.org/10.3390/chemosensors4040025.
[74] S.-M. Li, Y.-S. Wang, S.-T. Hsiao, W.-H. Liao, C.-W. Lin, S.-Y. Yang, H.-W. Tien, C.-C.M. Ma, C.-C. Hu, Fabrication of a silver nanowire-reduced graphene oxide-based electrochemical biosensor and its enhanced sensitivity in the simultaneous determination of ascorbic acid, dopamine, and uric acid, J. Mater. Chem. C. 3 (2015) 9444–9453, https://doi.org/10.1039/C5TC01564B.
[75] P. Fanjul-Bolado, D.H. Santos, V.M. Montoya, A. Costa-García, Uric acid determination by adsorptive stripping voltammetry on multiwall carbon nanotubes based screen-printed electrodes, Electroanalysis 27 (2015) 1276–1281, https://doi.org/10.1002/elan.201400690.
[76] S. Piermarini, D. Migliorelli, G. Volpe, R. Massoud, A. Pierantozzi, C. Cortese, G. Palleschi, Uricase biosensor based on a screen-printed electrode modified with Prussian blue for detection of uric acid in human blood serum, Sensor. Actuator. B Chem. 179 (2013) 170–174, https://doi.org/10.1016/j.snb.2012.10.090.
[77] P. Kanyong, R.M. Pemberton, S.K. Jackson, J.P. Hart, Development of a sandwich format, amperometric screen-printed uric acid biosensor for urine analysis, Anal. Biochem. 428 (2012) 39–43, https://doi.org/10.1016/j.ab.2012.05.027.
[78] J. Ping, J. Wu, Y. Wang, Y. Ying, Simultaneous determination of ascorbic acid, dopamine and uric acid using high-performance screen-printed graphene electrode, Biosens. Bioelectron. 34 (2012) 70–76, https://doi.org/10.1016/j.bios.2012.01.016.
[79] S.-H. Huang, H.-H. Liao, D.-H. Chen, Simultaneous determination of nor-epinephrine, uric acid, and ascorbic acid at a screen printed carbon electrode modified with polyacrylic acid-coated multi-wall carbon nanotubes, Biosens. Bioelectron. 25 (2010) 2351–2355, https://doi.org/10.1016/j.bios.2010.03.028.
[80] J.-M. Zen, Y.-Y. Lai, H.-H. Yang, A. Senthil Kumar, Multianalyte sensor for the simultaneous determination of hypoxanthine, xanthine and uric acid based on a preanodized nontronite-coated screen-printed electrode, Sensor. Actuator. B Chem. 84 (2002) 237–244, https://doi.org/10.1016/S0925-4005(02)00031-X.
[81] M.A.T. Gilmartin, J.P. Hart, Novel, reagentless, amperometric biosensor for uric acid based on a chemically modified screen-printed carbon electrode coated with cellulose acetate and uricase, Analyst 119 (1994) 833, https://doi.org/10.1039/an9941900833.
[82] M.A.T. Gilmartin, J.P. Hart, B. Birch, Voltammetric and amperometric behaviour of uric acid at bare and surface-modified screen-printed electrodes: studies towards a disposable uric acid sensor, Analyst 117 (1992) 1299, https://doi.org/10.1039/an9921701299.
[83] W. Rosner, S.E. Hankinson, P.M. Sluss, H.W. Vesper, M.E. Wierman, Challenges to the measurement of estradiol: an endocrine society position statement, J. Clin. Endocrinol. Metab. 98 (2013) 1376–1387, https://doi.org/10.1210/jc.2012-3780.
[84] B. Elliott, C. Muir, D. DeCatanzaro, Sources of variance within and among young men in concentrations of 17β-estradiol and testosterone in axillary perspiration, Physiol. Behav. 173 (2017) 23–29, https://doi.org/10.1016/j.physbeh.2017.01.036.
[85] C. Muir, K. Treasurywala, S. McAllister, J. Sutherland, L. Dukas, R. Berger, A. Khan, D. DeCatanzaro, Enzyme immunoassay of testosterone, 17β-estradiol, and progesterone in perspiration and urine of preadolescents and young adults: exceptional levels in men's axillary perspiration, Horm. Metab. Res. 40 (2008) 819–826, https://doi.org/10.1055/s-0028-1082042.
[86] R.M. Pemberton, T.T. Mottram, J.P. Hart, Development of a screen-printed carbon electrochemical immunosensor for picomolar concentrations of estradiol in human serum extracts, J. Biochem. Biophys. Methods 63 (2005) 201–212, https://doi.org/10.1016/j.jbbm.2005.05.002.
[87] I. Ojeda, J. López-Montero, M. Moreno-Guzmán, B.C. Janegitz, A. González-Cortés, P. Yáñez-Sedeño, J.M. Pingarrón, Electrochemical immunosensor for rapid and sensitive determination of estradiol, Anal. Chim. Acta 743 (2012) 117–124, https://doi.org/10.1016/j.aca.2012.07.002.
[88] Y. Wang, J. Luo, J. Liu, X. Li, Z. Kong, H. Jin, X. Cai, Electrochemical integrated paper-based immunosensor modified with multi-walled carbon nanotubes nanocomposites for point-of-care testing of 17β-estradiol, Biosens. Bioelectron. 107 (2018) 47–53, https://doi.org/10.1016/j.bios.2018.02.012.
[89] S.C. Wang, K.S. Chang, C.J. Yuan, Enhancement of electrochemical properties of screen-printed carbon electrodes by oxygen plasma treatment, Electrochim. Acta 54 (2009) 4937–4943, https://doi.org/10.1016/j.electacta.2009.04.006.
[90] F. Ghamouss, E. Luais, C. Thobie-Gautier, P.-Y. Tessier, M. Boujtita, Argon plasma treatment to enhance the electrochemical reactivity of screen-printed carbon surfaces, Electrochim. Acta 54 (2009) 3026–3032, https://doi.org/10.1016/j.electacta.2008.12.011.
[91] A.P. Washe, P. Lozano-Sánchez, D. Bejarano-Nosas, I. Katakis, Facile and versatile approaches to enhancing electrochemical performance of screen printed electrodes, Electrochim. Acta 91 (2013) 166–172, https://doi.org/10.1016/j.electacta.2012.12.110.
[92] H. Wei, J.-J. Sun, Y. Xie, C.-G. Lin, Y.-M. Wang, W.-H. Yin, G.-N. Chen, Enhanced electrochemical performance at screen-printed carbon electrodes by a new pretreating procedure, Anal. Chim. Acta 588 (2007) 297–303, https://doi.org/10.1016/j.aca.2007.02.006.
[93] G. Cui, J.H. Yoo, J.S. Lee, J. Yoo, J.H. Uhm, G.S. Cha, H. Nam, Effect of pretreatment on the surface and electrochemical properties of screen-printed carbon paste electrodes, Analyst 126 (2001) 1399–1403, https://doi.org/10.1039/b102934g.
[94] R. Gusmão, V. López-Puente, I. Pastoriza-Santos, J. Pérez-Juste, M.F. Proença, F. Bento, D. Geraldo, M.C. Paiva, E. González-Romero, Enhanced electrochemical sensing of polyphenols by an oxygen-mediated surface, RSC Adv. 5 (2015) 5024–5031, https://doi.org/10.1039/C4RA12660B.
[95] J. Wang, Z. Xu, M. Zhang, J. Liu, H. Zou, L. Wang, Improvement of electrochemical performance of screen-printed carbon electrodes by UV/ozone modification, Talanta 192 (2019) 40–45, https://doi.org/10.1016/j.talanta.2018.08.065.
[96] M.D. Osborne, B.J. Seddon, R.A.W. Dryfe, G. Lagger, U. Loyall, H. Schäfer, H.H. Girault, Excimer laser-induced electrochemical activity in carbon ink films, J. Electroanal. Chem. 417 (1996) 5–15, https://doi.org/10.1016/S0022-0728(96)04781-X.
[97] J. Wang, M. Pedrero, H. Sakslund, O. Hammerich, J. Pingarron, Electrochemical activation of screen-printed carbon strips, Analyst 121 (1996) 345, https://doi.org/10.1039/an9962100345.
[98] L.-S. Johansson, J. Campbell, K. Koljonen, P. Stenius, Evaluation of surface lignin on cellulose fibers with XPS, Appl. Surf. Sci. 144–145 (1999) 92–95, https://doi.org/10.1016/S0169-4332(98)00920-9.
[99] M. Sevilla, A.B. Fuertes, The production of carbon materials by hydrothermal carbonization of cellulose, Carbon N. Y. 47 (2009) 2281–2289, https://doi.org/10.1016/j.carbon.2009.04.026.
[100] Xpssimplified.com., XPS Interpretation Of Carbon, n.d. Available at https://xpssimplified.com/elements/carbon.php , Accessed date: 12 August 2019.
[101] L.J. Kepley, A.J. Bard, Ellipsometric, electrochemical, and elemental characterization of the surface phase produced on glassy carbon electrodes by electrochemical activation, Anal. Chem. 60 (1988) 1459–1467, https://doi.org/10.1021/ac00165a022.
[102] T.R. Ray, J. Choi, A.J. Bandodkar, S. Krishnan, P. Gutruf, L. Tian, R. Ghaffari, J.A. Rogers, Bio-Integrated wearable systems: a comprehensive review, Chem. Rev. 119 (2019) 5461–5533, https://doi.org/10.1021/acs.chemrev.8b00573.